Reflection of sound from random distributions of semi-cylinders on a hard plane: models and data

Patrice Boulanger[1], Keith Attenborough[1*], Qin Qin[1] and Chris M Linton[2]
[1] Department of Engineering, The University of Hull, Hull HU6 7RX, United Kingdom
[2] Department of Mathematical Sciences, Loughborough University, Leicestershire LE11 3TU, United Kingdom

ABSTRACT
A new analytical theory for multiple scattering of cylindrical acoustic waves by an array of finite impedance semi-cylinders embedded in a smooth acoustically hard surface is derived by extending previous results for plane waves [Linton and Martin, J. Acoust. Soc. Am. **117** (6) 3413 – 3423 (2005)]. Although the computational demands of the new theory increase as the number of the semi-cylinders in the arrays and/or the frequency increases, the theory offers an improvement on analytical boss theories since the latter (i) are restricted to non-deterministic (infinite) random distributions of semi-cylinders with spacing/radii small compared to the incident wavelength and (ii) are derived only for plane waves. The influence on prediction accuracy of truncation of the infinite system of equations introduced by the new theory is explored empirically. Laboratory measurements have been made over deterministic random arrays of identical varnished wooden semi-cylinders on a glass plate. The agreement between predictions and measured relative Sound Pressure Level spectra is very good both for single deterministic random distributions and for averages representing non-deterministic random distributions. The analytical theory is found to give identical results to a Boundary Element calculation but is much faster to compute.

PACS numbers: 43.50.Vt, 43.28.En

1. Introduction

Surface roughness is known to have significant influence on near-grazing sound. One approach to modeling long wavelength sound reflection from randomly rough surfaces considers scattering from idealized roughness elements or 'bosses'. Several measurements have been made of relative sound pressure level (SPL) spectra above rough surfaces, where the roughness height and spacing are small compared to the wavelengths of interest [1-5]. These data have been compared with predictions of models derived by Attenborough and Taherzadeh [1] from a boss theory by Tolstoy [6],[7]. It has been found necessary to adjust the impedance of the scatterers and imbedding plane to obtain good agreement between predictions based on Tolstoy's boss theory and the data. Tolstoy's effective admittance models [6],[7] predict that a surface wave is generated at grazing-incidence above a hard rough boundary and that the effective admittance above a hard rough boundary is purely imaginary. However, comparison with data [2] indicates that Tolstoy-based predictions overestimate the surface wave component, especially at grazing incidence, and that it is necessary to include attenuation due to non-specular scatter to obtain a good fit with these data [4]. In other comparisons of predictions and data [5], the assumed location of the effective admittance plane has been adjusted to improve agreement with data at higher frequencies. Poor agreement between laboratory measurements of propagation over rough convex surfaces and

* corresponding author: e-mail k.attenborough@hull.ac.uk

predictions based on the Tolstoy effective admittance formulation has been found [4] and it has been suggested that the absence of a real part of admittance corresponding to non-specular scattering effects might be responsible for this. Non-specular scattering is particularly important for random roughness [1]. The theory of Lucas and Twersky [8] incorporates non-specular scattering and resulting expressions have been used to model 2-D periodic and random hard roughness elements, giving reasonable agreement with measured short-range ground effect [9]. A heuristic extension of this model to sound reflection from rough surfaces of finite impedance has given predictions in tolerable agreement with ground effect measured over rough surfaces in the laboratory and outdoors [10]. However, the real part of the effective impedance obtained from Lucas and Twersky's theory for hard rough surfaces does not have the dominant real part low frequency limit that is expected from physical considerations [11]. Measurements of complex relative sound pressure level over porous roughness on a flat hard surface have been reported [12], and effective impedance spectra have been obtained from these measurements by numerical solution of the complex admittance equation [13] obtained from the classical expression for a point source over an impedance boundary. It is found that predictions of Twersky's theory [14] do not agree at low frequencies with measured data for rough porous surfaces. Therefore, a new theory is needed that improves modeling of low frequency effective impedance.

This work presents an analytical theory for long-wavelength plane or cylindrical acoustic waves scattered by a finite array of finite impedance semi-cylinders embedded in a smooth hard surface. The derivation is based on the method used by Linton *et al* [17] for the problem of *plane* wave scattering by finite arrays of hard cylinders in water. Subsequent work [18] has yielded results for identical finite impedance cylinders. Initially, this work extends the plane wave results to an array of cylinders characterized by different radii and finite impedances. Subsequently, the problem of plane waves incident on semi-cylinders embedded in a smooth hard surface is considered. Further developments model the scattering of long-wavelength *cylindrical* waves incident on finite impedance semi-cylinders embedded in a smooth hard surface. Predictions are compared to data for relative sound pressure level spectra measured over wooden semi-cylindrical roughness elements on a glass plate.

Section 2.1 presents a solution for plane acoustic waves scattered by a finite array of finite impedance semi-cylinders embedded in a smooth hard surface. This section presents also the main results from Twersky's theory. Section 2.2 presents a solution for the field resulting when cylindrical acoustic waves are scattered by a finite array of finite impedance semi-cylinders embedded in a smooth hard surface. The Boundary Element Model (BEM), to which the new theory is compared, is introduced briefly. Section 2.3 establishes an empirical relationship for the frequency dependence of the truncation parameter used to solve the infinite number of equations involved in the theory. Section 2.4 summarizes the theory involved to model the complex compressibility and wave-number and hence the surface impedance of rigid-porous semi-cylinders. Section 3 describes the experimental procedures. Section 4.1 compares laboratory measurements of complex relative sound pressure level (SPL) over random deterministic distributions of wooden semi-cylinders on a glass plate with predictions from the new theory and Twersky's theory. Comparisons with BEM calculations are presented in 4.2. Section 4.3 compares average measured relative SPL spectra representative of a given roughness density to average predictions from the new theory. Measured data reported previously [9] are revisited and compared to new predictions. Conclusions are drawn in section 5.

2. THEORETICAL FORMULATIONS

2.1 Scattering of plane waves by an array of porous semi-cylinders distributed on a hard plane

2.1.1. Extension of Linton's theory Linton *et al* [17,18] have studied scattering of plane waves incident on finite arrays of identical hard and finite impedance cylinders. Consider an array of N non-identical semi-cylinders. The polar coordinates of the field point in the Cartesian reference frame (Ox, Oy) are represented by (r, θ), and the polar coordinates of the field point in the

reference frame (O_jx, O_jy) centered at the j^{th} semi-cylinder center O_j (x_j, y_j) are represented by (r_j, θ_j) (see Figure 1). Exterior to the semi-cylinders the pressure field, P, satisfies

$$\nabla^2 P + k^2 P = 0 \tag{1}$$

and interior to the semi-cylinder j, the pressure field, P_j, satisfies

$$\nabla^2 P_j + k_j^2 P_j = 0\,. \tag{2}$$

k and k_j are the wave-numbers outside and inside the semi-cylinders respectively.

The scattered term P_{scat} can be decomposed into a sum of the contributions from the N semi-cylinders. The scattering contribution from the j^{th} semi-cylinder is sought in the form of a cylindrical wave which can be expanded using the basis function set $e^{in\theta_j}$ for the polar angle contribution and Hankel functions of the first kind and order n, $H_n(kr_j)$, for the radial coordinates. The total scattered wave is written as

$$P_{scat} = \sum_{j=1}^{N} \sum_{n=-\infty}^{\infty} A_n^j Z_n^j H_n(kr_j) e^{in\theta_j}\,. \tag{3}$$

The solution to equation (2) is sought in the form

$$P_j = \sum_{n=-\infty}^{\infty} B_n^j J_n(k_j r_j) e^{in\theta_j} \tag{4}$$

where $J_n(k_j r_j)$ is the Bessel function of the first kind and order n. The coefficients A_n^j and B_n^j needed for the solution of equations (1) and (2) are determined from the boundary conditions. The coefficients Z_n^j are chosen for later convenience to be

$$Z_n^j = \frac{q_j J_n'(ka_j) J_n(k_j a_j) - J_n(ka_j) J_n'(k_j a_j)}{q_j H_n'(ka_j) J_n(k_j a_j) - H_n(ka_j) J_n'(k_j a_j)}. \tag{5}$$

Equation (5) allows for cylinders having different radii and impedances. The coefficients q_j are defined as $q_j = \dfrac{\rho_j c_j}{\rho_0 c_0}$ where ρ_j and c_j represent the density of fluid and the sound speed inside the j^{th} cylinders respectively. ρ_0 and c_0 are the density of air and the sound speed outside the cylinder. The limit $q_j \to \infty$ can be used to model acoustically hard semi-cylinders. J'_n and H'_n are the derivatives of the Bessel and Hankel functions of the first kind respectively and a_j is the radius of the j^{th} cylinder. Graf's addition theorem [22] for Bessel functions is used to express $H_n(kr_j)$ in terms of coordinates (r_s, θ_s) needed for the boundary conditions at the surface of cylinder s, and equation (3) becomes

$$P_{scat} = \sum_{n=-\infty}^{\infty} A_n^s Z_n^s H_n(kr_s) e^{in\theta_s} + \sum_{j=1,\, j\neq s}^{N} \sum_{n=-\infty}^{\infty} A_n^j Z_n^j \sum_{m=-\infty}^{m=\infty} J_m(kr_s) H_{n-m}(kR_{js}) e^{im\theta_s} e^{i(n-m)\alpha_{js}} \tag{6}$$

where α_{js} is 0 or π depending on the respective positions of the j^{th} and s^{th} semi-cylinders. This equation is valid provided $r_s < R_{js}$ where R_{js} is the distance between the centers of cylinders j and s. A plane wave

$$P_{in} = e^{i\vec{k}\cdot\vec{r}} = e^{ikr\cos(\theta-\beta)} \tag{7}$$

is assumed to be incident at angle β with respect to the +x-axis on an array of N infinitely long semi-cylinders embedded in a smooth surface (Figure 1). The propagation vector $\vec{k}$ is considered to be perpendicular to the cylinder axes. When applying the boundary conditions, it is useful to express the incident wave in terms of the radial position r_j of the j^{th} semi-cylinder and the polar

angle θ_j. Writing $\vec{r} = \overrightarrow{OO_j} + \vec{r}_j$, the dot product $\vec{k} \cdot \vec{r}$ enables expression of the incident plane wave equation (7) as

$$P_{in} = I_j e^{ikr_j \cos(\theta_j - \beta)} \tag{8}$$

where I_j is a phase factor associated with semi-cylinder *j* defined as $I_j = e^{ikx_j \cos\beta}$.

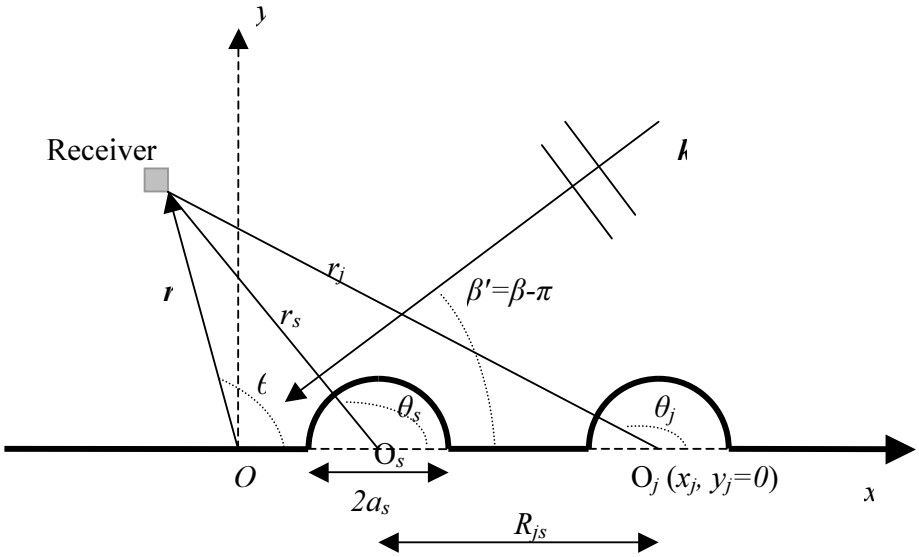

Figure 1 Cross-sections of two semi-cylinders and the geometry used in developing the theory for plane waves.

To develop an expression for the wave scattered by a finite array of non-identical finite impedance semi-cylinders embedded in a smooth hard surface, the effect of the hard embedding plane is taken into account by assuming a reflected plane wave

$$P_{ref} = e^{ikr\cos(\theta+\beta)}. \tag{9}$$

This is the mirror reflection of the incident wave in the plane containing the semi-cylinder axes. In terms of r_j and θ_j, the reflected wave (9) is

$$P_{ref} = I_j e^{ikr_j \cos(\theta_j + \beta)} \tag{10}$$

The sum of the incident and reflected waves can be expanded as [21]

$$P_{in} + P_{ref} = 2I_j \sum_{n=-\infty}^{+\infty} J_n(kr_j) e^{in(\pi/2+\theta_j)} \cos(n\beta).$$

Thus the total field $P = P_{in} + P_{ref} + P_{scat}$ can be written as

$$P = 2I_j \sum_{n=-\infty}^{+\infty} J_n(kr_j) e^{in(\pi/2+\theta_j)} \cos(n\beta) + \sum_{n=-\infty}^{\infty} A_n^s Z_n^s H_n(kr_s) e^{in\theta_s}$$
$$+ \sum_{j=1, j\neq s}^{N} \sum_{n=-\infty}^{\infty} A_n^j Z_n^j \sum_{m=-\infty}^{m=\infty} J_m(kr_s) H_{n-m}(kR_{js}) e^{im\theta_s} e^{i(n-m)\alpha_{js}}. \tag{11}$$

The boundary condition $P\big|_{r_s=a_s} = P_s\big|_{r_s=a_s}$ on the s^{th} semi-cylinder leads to expressions for the coefficients B_n^j in terms of A_n^j. After substituting this result in (11), the other boundary condition, $\frac{1}{\rho_0}\frac{\partial P}{\partial r_s}\Big|_{r_s=a_s} = \frac{1}{\rho_s}\frac{\partial P_s}{\partial r_s}\Big|_{r_s=a_s}$, gives the infinite system of equations

$$A_m^s + \sum_{\substack{j=1 \\ j\neq s}}^{N}\sum_{n=-\infty}^{\infty} A_n^j Z_n^j H_{n-m}\left(kR_{js}\right)e^{i(n-m)\alpha_{js}} = -2\cos(m\beta)I_s e^{im\pi/2},\ m\in \mathrm{Z},\ s=1, \ldots, \mathrm{N}. \quad (12)$$

Note that the restriction $r_s < R_{js}$ due to the use of Graf's addition theorem is met at the surface of the cylinders where the boundary conditions are applied.

To evaluate the unknowns A_n^j, the infinite system (12) is truncated to a system of $N(2M+1)$ equations

$$A_m^s + \sum_{\substack{j=1 \\ j\neq s}}^{N}\sum_{n=-M}^{M} A_n^j Z_n^j H_{n-m}\left(kR_{js}\right)e^{i(n-m)\alpha_{js}} = -2\cos(m\beta)I_s e^{im\pi/2},\ m=-M, \ldots +M,\ s=1,\ldots N. \quad (13)$$

This system is solved numerically by using the IMSL routine DLSACG [19] once an appropriate value of truncation parameter M is chosen. Section II.C addresses the method used to choose the truncation parameter. When the coefficients A_n^j are known, equation (3) together with (5) is used to compute the total pressure. Henceforth equations (3) through (13) are called the 'new theory'.

2.1.2 Twersky's theory for parallel porous semi-cylindrical elements in a flat hard surface The 'boss' theory derived from Twersky's work [14] is detailed elsewhere [12]. Only the main results are reported here. Consider circular semi-cylindrical roughness elements with radius a and with their axes along the y-direction (see Figure 2).

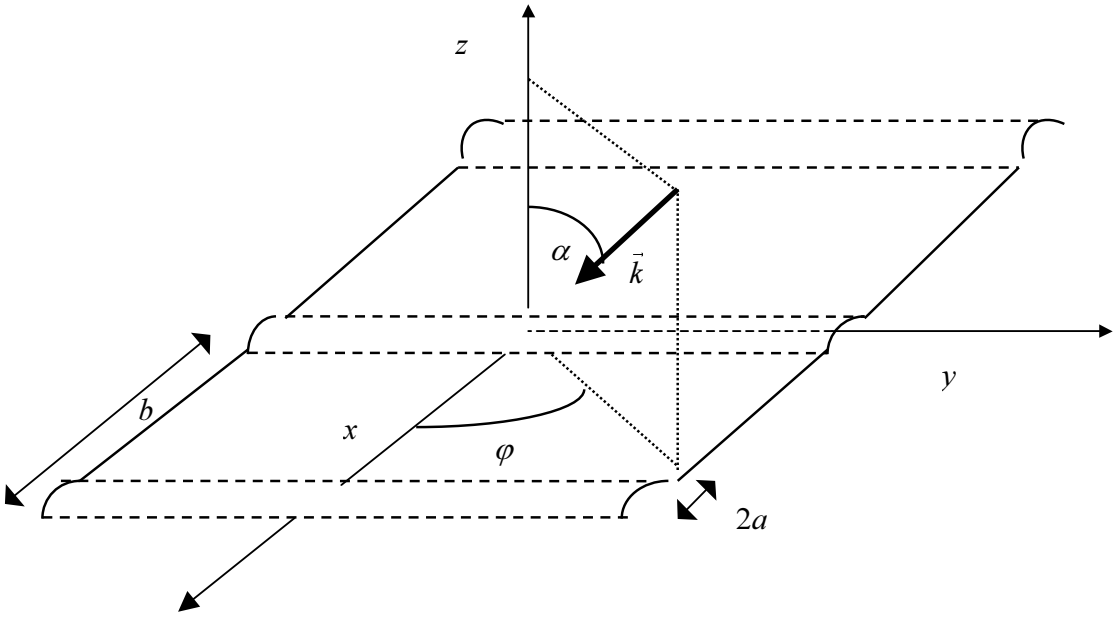

Figure 2 A plane wave incident on a surface containing a grating of semi-cylinders.

When the azimuthal angle φ is zero and the plane-wave incidence angle α is measured from the vertical axis z, the effective admittance β_{rough} relative to air of a hard plane containing randomly spaced 2-D porous circular semi-cylinders is

$$\beta_{\text{rough}} = \eta - i\xi. \tag{14}$$

where

$$\xi = kV\left\{C_1 - \text{Re}\left[\frac{B-1}{1+(B-1)Q_2}\right]\sin^2\alpha\right\} \tag{15}$$

and

$$\eta = kV\left\{C_2 - \text{Im}\left[\frac{B-1}{1+(B-1)Q_2}\right]\sin^2\alpha\right\} + k^3(1-W)^2\frac{V^2}{2n}\left\{C_1^2 + \frac{1}{2}\text{Re}\left[\frac{B-1}{1+(B-1)Q_2}\right]^2\sin^2\alpha\right\}. \tag{16}$$

The raised cross sectional area per unit length is $V = n\pi a^2/2$, where n the number of semi-cylinders per unit length. For circular semi-cylinders [14], $Q_2 = \frac{1}{2} - \frac{I_2 a^2}{2b^{*2}}$ where

$$I_2 \cong 2W\left(1 + 0.307W + 0.137W^2\right) \qquad \text{for } W < 0.8, \tag{17a}$$

$$I_2 \cong \frac{\pi^2}{3}\left[1 - \frac{2(1-W)}{W}\right] + 6\frac{(1-W)^2}{W^2}\left[\frac{\pi^2}{6} + 1.202\right] \qquad \text{for } W \geq 0.8, \tag{17b}$$

The packing density of the distribution of roughness elements $W = nb^* = \frac{b^*}{b}$, where b is the average roughness separation distance and b^* is the size of the exclusion region around any scatterer, i.e. is the minimum distance between the centers of adjacent roughness elements. Note that the theory [14] is based on the approximations $ka \ll 1$ and $kb^* < 1$. If the roughness elements considered are non-porous, rigid and on a rigid base plane, the relative inverse mass density ratio B, which is the density of air divided by the complex density of air in the semi-cylinder pores, $\to 0$. In addition, since the relative compressibility $\kappa \to 0$ and $C_1 + iC_2 = \kappa - 1$, $C_1 = -1$ and $C_2 = 0$. If P is the total (complex) pressure at the receiver due to a point source above an homogeneous impedance plane and $P_1 = P_0\frac{e^{ikR_1}}{R_1}$ is the pressure due to the direct wave from the source (assuming time dependence $\exp(-i\omega t)$), then

$$\text{relative SPL} = 20\lg\left|\frac{P}{P_1}\right| \tag{18}$$

According to the classical theory for the sound field due to a point source above an impedance boundary [23],

$$P = P_0\frac{e^{ikR_1}}{R_1} + QP_0\frac{e^{ikR_2}}{R_2}. \tag{19}$$

Q, the spherical wave reflection coefficient, is defined by $Q = R + [1-R]F(w)$, where $F(w) = 1 + i\sqrt{\pi}we^{-w^2}erfc(-iw)$, R is the plane wave reflection coefficient, R_1 is the direct path

length from source to receiver, R_2 is the path length through the specular reflection point, P_0 is a constant and $w = \sqrt{\frac{1}{2}ikR_2}\left(\beta + \cos\alpha\right)$. For a locally- reacting surface, the plane wave reflection coefficient is defined by

$$R = \frac{\cos\alpha - \beta}{\cos\alpha + \beta} \ . \tag{20}$$

In this work, the relative SPL is computed from Twersky's theory by inserting (16), for the rough surface admittance β_{rough}, into (20) and (19).

2.2. Cylindrical waves scattered by parallel finite impedance semi-cylinders elements in a hard plane

2.2.1. Analytical Theory Consider a cylindrical wave incident from a single source on an array of N different finite impedance semi-cylinders embedded in a flat hard surface. The Helmholtz equations (1) and (2) are solved using the same coordinate system as used for plane waves. The incident pressure amplitude can be written

$$P_{in}=H_0\,(k\rho_1) \tag{21}$$

where ρ_1 is the source receiver distance (see Figure 3). It is useful for subsequent development to express $H_0\,(k\rho_1)$ in terms of the coordinates (r_s, θ_s) by using Graf's addition theorem [22]:

$$P_{in} = \sum_{n=-\infty}^{+\infty} J_n\left(kr_s\right)H_n\left(kS_{s1}\right)e^{-in\sigma_{s1}}e^{in\theta_s} \tag{22}$$

with the restriction $r_s < S_{s1}$, where S_{s1} is the radial distance between the cylinder center s and the source 1. To develop an expression for the wave scattered by a finite array of non-identical finite impedance semi-cylinders embedded in a smooth hard surface, the effect of the hard surface embedding the semi-cylinders is taken into account by assuming an image source and hence a reflected wave

$$P_{ref}=H_0\,(k\rho_2) \tag{23}$$

where ρ_2 is the image-source/receiver distance (see Figure 3).

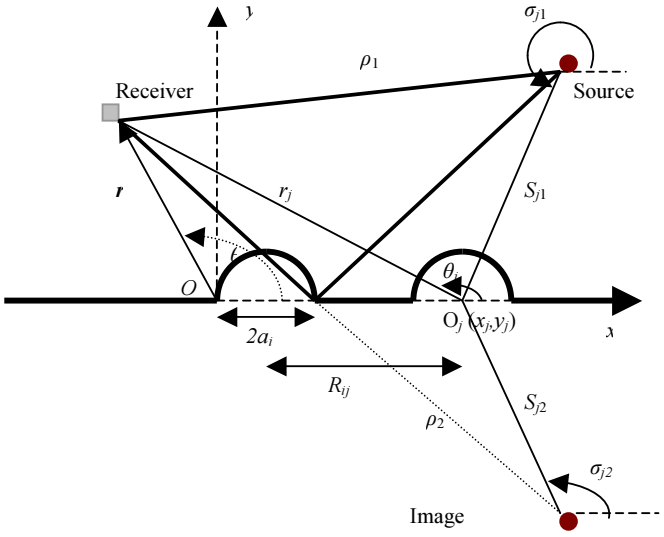

Figure 3 Cross-sections of two semi-cylinders and geometry used in the theory developed for a line source.

If the reflected wave (23) is expressed in terms of r_s and θ_s as in (22), the total field outside the semi-cylinders becomes

$$P = \sum_{n=-\infty}^{+\infty} J_n(kr_s)e^{in\theta_s}\left[H_n(kS_{s1})e^{-in\sigma_{s1}} + H_n(kS_{s2})e^{-in\sigma_{s2}}\right] + \sum_{n=-\infty}^{\infty} A_n^s Z_n^s H_n(kr_s)e^{in\theta_s} + \sum_{j=1,\, j\neq s}^{N}\sum_{n=-\infty}^{\infty} A_n^j Z_n^j \sum_{m=-\infty}^{m=\infty} J_m(kr_s)H_{n-m}(kR_{js})e^{im\theta_s}e^{i(n-m)\alpha_{js}} \quad (24)$$

provided that $r_s < S_{s1}$ and $r_s < S_{s2}$.

The solution to the Helmholtz equation (2) is sought in the form of the pressure field (4) inside the semi-cylinders. The boundary conditions are as before and, after some algebra, lead to the infinite system of equations

$$A_m^s + \sum_{\substack{j=1\\ j\neq s}}^{N}\sum_{n=-\infty}^{\infty} A_n^j Z_n^j H_{n-m}(kR_{js})e^{i(n-m)\alpha_{js}} = -H_m(kS_{p1})e^{-im\sigma_{p1}} - H_m(kS_{p2})e^{-im\sigma_{p2}} \quad (25)$$

with unknowns A_n^j and $m \in$ Z, s=1,..., N. Note that the restrictions $r_s < S_{s1}$ and $r_s < S_{s2}$ due to Graf's addition theorem applied to the source terms, are met at the surface of the cylinders where the boundary conditions are applied. To evaluate the coefficients A_n^j, the infinite system of equations (26) is truncated to a system of $N(2M+1)$ equations

$$A_m^s + \sum_{\substack{j=1\\ j\neq s}}^{N}\sum_{n=-M}^{M} A_n^j Z_n^j H_{n-m}(kR_{js})e^{i(n-m)\alpha_{js}} = -H_m(kS_{p1})e^{-im\sigma_{p1}} - H_m(kS_{p2})e^{-im\sigma_{p2}} \quad (26)$$

with $m = -M, \ldots.+M$ and $s = 1,\ldots..,$ N. The system of equations (26) is solved numerically using the IMSL routine DLSACG [19] once the appropriate choice of the truncation parameter M has been made. Section II.C addresses the method used to choose the truncation parameter. Note that only the right hand side of (26) differs from the result (13) for plane waves.

2.2.2. The Boundary Element Model Chandler-Wilde [24,25] has developed a boundary integral equation method for solving the Helmholtz equation for the pressure at the receiver due to a line source above an impedance plane. The resulting boundary integral equation is solved approximately by assuming a constant pressure over each boundary element of the ground surface and using the (point) collocation method. The latter approximates the solution by weighted residuals and sets the residual function to zero at a series of points. These equations for each point plus the discretization of the integral equation give a system of equations whose dimension is the number of collocation points. It is possible to model either a flat or a profiled ground surface since the discretizing points can be chosen out of the horizontal plane. To save computation time, an equivalent two-dimensional problem is solved i.e. only ground and sound sources are modeled that show no variation along one axis. Source, receiver and specular reflection point are assumed to be in a vertical plane perpendicular to the roughness axis, and a line integral is solved instead of a surface integral. The acoustic impedance can be chosen independently for each surface element of the profile. The BEM is used to predict the relative SPL over rough surfaces by including the roughness profile in the form of node coordinates input to the program. Acoustically-hard surfaces are modeled by setting the admittance $\beta = 0$.

2.2 3. Influence of the truncation parameter value The effects of the value of the truncation parameter M on the accuracy of the relative SPL spectra predicted for a given random distributions of semi-cylinders may be investigated empirically. The relative SPL spectra are computed from

$$20\lg\left|\frac{P_{in}+P_{ref}+P_{scat}}{P_{in}}\right|. \quad (27)$$

Several relative SPL spectra have been obtained for a fixed random distribution of *five* acoustically hard semi-cylinders as M is varied from 1 to 7. Row 1 of Table 1 is deduced from these spectra and shows the frequency f at which the spectrum obtained for truncation parameter M departs significantly from that obtained for $M = 7$. Table 1 suggests, for example, that $M = 1$ could be used for $f < 3.4$ kHz, $M = 2$ could be used for $f < 5.5$ kHz etc. Since the spectra predicted for values of M between 5 and 7 are identical in the frequency range 0.2 – 10 kHz, it seems that $M = 5$ avoids any truncation error up to 10 kHz for calculations involving 5 semi-cylinders. Effects of the variation of M on the relative SPL spectra obtained for a given random distributions of *seven* acoustically hard semi-cylinders are summarized in row 2 of Table 1. It shows the frequency at which the spectrum obtained for a given value of truncation parameter M departs from that obtained for $M = 6$. As the spectra predicted for $M = 5$ and 6 are identical in the frequency range 0.2 – 10 kHz, it seems that $M = 5$ avoids any truncation error up to 10 kHz for calculations involving 7 semi-cylinders also.

Table 1: Upper frequency bounds of validity corresponding to the given truncation parameter value for a random distribution of five and seven semi-cylinders

M	**1**	**2**	**3**	**4**
Upper f (kHz) 5 cylinders	3.4	5.5	6.6	9
Upper f (kHz) 7 cylinders	3.0	5.6	6.5	9

Since the results in Row 2 of Table 1 are very similar to those in row 1, it seems that the frequency thresholds of the truncation parameters are fairly independent of the number of semi-cylinders and the random distributions used. Consequently, these results will be used in the following work for various numbers and distributions of semi-cylinders. Although, in principle, the theory is valid for all wavelengths, the use of a truncation parameter means that there is an frequency beyond which model is invalid and this is determined by the truncation parameter value. Nevertheless, it will be shown in section IV that satisfactory agreement with measured data has been obtained up to 25 kHz and that complete numerical agreement is found with BEM calculations up to 20 kHz.

2.2.4. The tortuous slit-pore model for rigid-porous materials Porous roughness elements can be included in the new theory through the use of the coefficients Z_n^j defined in equation (5). For simplicity, although more sophisticated models for the acoustical properties of arbitrary rigid-porous materials are available [15], the pores in the roughness elements are considered to be identical tortuous slits. It should be noted that, for a given flow resistivity and porosity, pore shape has little influence on the surface impedance [16]. In a medium with flow resistivity R_s, porosity Ω, fluid density ρ and tortuosity T, and assuming time dependence $\exp(-i\omega t)$, the effective relative compressibility $C(\omega)$ is given by

$$C(\omega)=\frac{1}{\rho_0 c_0^2}\left\{\gamma-(\gamma-1)\left[1-\frac{\tanh(\lambda\sqrt{-iN_{PR}})}{\lambda\sqrt{-iN_{PR}}}\right]\right\} \quad (28)$$

where the dimensionless parameter $\lambda=\left(\frac{3\rho_0\omega T}{\Omega R_S}\right)^{1/2}$, $\gamma=C_p/C_v$ is the ratio of specific heat at constant pressure of the gas to the specific heat at constant volume and $\omega=2\pi f$ is the angular frequency. The mass density is given by

$$\rho(\omega)=\frac{T}{\Omega}\rho_0\left[1-\frac{\tanh(\lambda\sqrt{-i})}{\lambda\sqrt{-i}}\right]^{-1}, \tag{29}$$

and the wave number inside the pores of the s^{th} semi-cylinder is

$$k_s=\omega\left(T_s\rho_s(\omega)C_s(\omega)\right)^{1/2}. \tag{30}$$

Consequently, for porous semi-cylinders, the arguments $k_s a_s$ of the integer order Bessel and Hankel functions and their derivatives that appear in (5) are complex.

3. Experiments

Measurements have been made of sound propagation from a point source over nine identical varnished wooden semi-cylinders of radius a = 0.01 m placed on a 0.006 m thick, square glass plate with sides of 0.76m. The source-receiver separation d was 0.7 m and source and receiver heights h were 0.07m. The semi-cylinders were randomly-spaced over a 49 cm wide area centered at the specular reflection point (see Figure 4) and with their axes normal to the source-receiver axis. The random semi-cylinder separations were normalized such that the sum of the separations was 31 cm (i.e. 49 – 9×2). Table 2 summarizes the values of intervals used, representing twenty deterministic random distributions of the semi-cylinders. More details of the experimental procedure are given elsewhere [12].

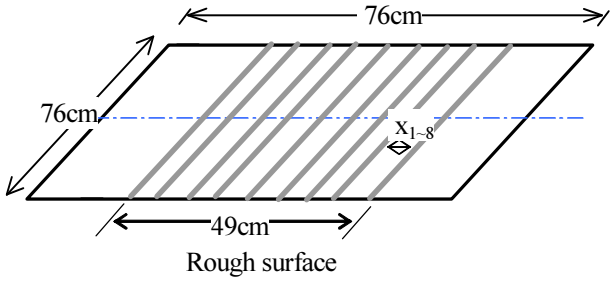

Figure 4 A distribution of nine semi-cylinders on a glass plate.

4. Comparisons between predictions and data

4.1. Predictions for individual random deterministic semi-cylinder distributions

Predictions have been made using (21) to (27) for semi-cylinder positions identical to that measured. Although data for twenty distributions are available, Figures 5, 6 and 7 show comparisons between measurements (thick solid line) and predictions for the first five distributions of hard semi-cylinders listed in Table 2.

Figure 5 shows the measured and predicted relative SPL spectra over the first random deterministic distribution of semi-cylinders according to the first line of Table 2. The dashed lines in Figures 5 and 6 show the predictions for rigid-porous semi-cylinders with flow resistivity R_s = 10^6 Pa.s.m^{-2}, porosity Ω = 0.1 and using equations (29) and (30) to compute the density of fluid and the sound speed inside the pores respectively. The dashed lines in Figures 7(a) and 7(b) show the predictions of Twersky's theory (equations (14) - (20)).

Table 2: Randomly-generated, normalized semi-cylinder separations

Distribution No	distance (cm)							
	x_1	x_2	x_3	x_4	x_5	x_6	x_7	x_8
1	2.9	1.3	5.6	5.8	6.0	3.9	4.6	1.0
2	3.1	4.9	6.2	1.9	1.8	6.0	1.6	5.6
3	8.8	2.3	2.3	0.5	0.8	6.2	1.9	8.2
4	1.7	1.7	9.7	4.3	3.3	3.1	3.5	3.8
5	7.0	4.4	0.2	6.0	4.5	5.2	0.7	3.1
6	3.4	6.4	4.2	2.3	3.4	4.2	1.1	5.9
7	2.5	3.4	7.9	6.7	0.7	1.1	3.4	5.1
8	3.3	3.7	0.7	5.3	4.5	4.7	4.8	4.0
9	2.6	7.6	3.0	6.0	0.5	3.2	4.4	3.8
10	1.8	6.2	3.6	5.2	3.0	6.8	0.5	3.9
11	4.4	2.6	3.8	4.8	0.5	5.7	5.5	3.6
12	3.8	1.8	4.2	0.3	4.0	4.9	6.7	5.2
13	0.9	3.8	5.6	4.6	6.8	6.5	0.4	2.4
14	4.5	6.3	5.2	4.5	3.1	0.7	4.3	2.3
15	3.1	4.3	4.1	5.2	3.7	5.6	3.6	1.4
16	2.8	4.4	4.9	2.8	2.9	4.6	5.9	2.6
17	5.8	3.7	4.1	1.5	3.5	6.0	2.2	4.2
18	4.5	4.7	5.5	5.0	2.2	3.7	4.3	1.2
19	5.2	3.7	1.9	5.8	6.9	3.5	0.1	3.9
20	3.2	7.0	0.0	2.3	0.4	5.4	5.0	7.6

For roughness distributions four and five, the minimum distances between two semi-cylinders (1.7cm and 0.2cm) shown in Table 2, indicate that the sizes of the exclusion regions (b^*) around any scatterer are ($2a$ + 1.7) cm and ($2a$ + 0.2) cm respectively. The twenty measured relative SPL spectra and the corresponding predictions are shown in Figures 8(a) and 8(b) respectively.

In contrast with the predictions of Twersky's theory (see Figure 7), the new theory's predictions are within 2 dB or less of most of the measured relative SPL spectra. However, the magnitudes of the ground effect dips are over predicted consistently by about 5dB. Nevertheless, typically, the ground effect dip frequency is predicted to within 1000 Hz of that measured. It should be noted also that the new theory predicts some of the measured spectral oscillations which result from interference between incident and scattered waves. According to Figures 5 and 6, the agreement between predicted and measured ground effect dip magnitudes is not improved if the semi-cylinders are modelled as slightly porous.

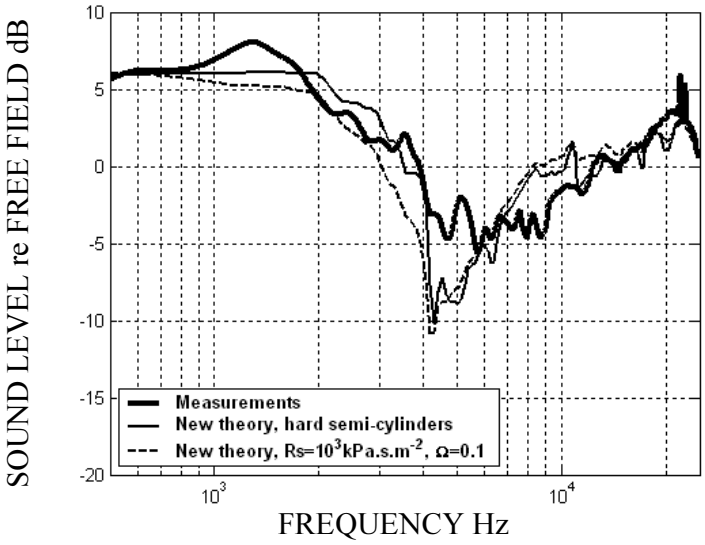

Figure 5 Predictions from the new theory for acoustically hard semi-cylinders (thin solid line), slightly porous (R_s =10^3 kPa.s.m^{-2}, Ω=0.1) semi-cylinders (dashed line), and measured (thick solid line) relative SPL spectra over the random distribution of nine semi-cylinders corresponding to row 1 in Table 2.

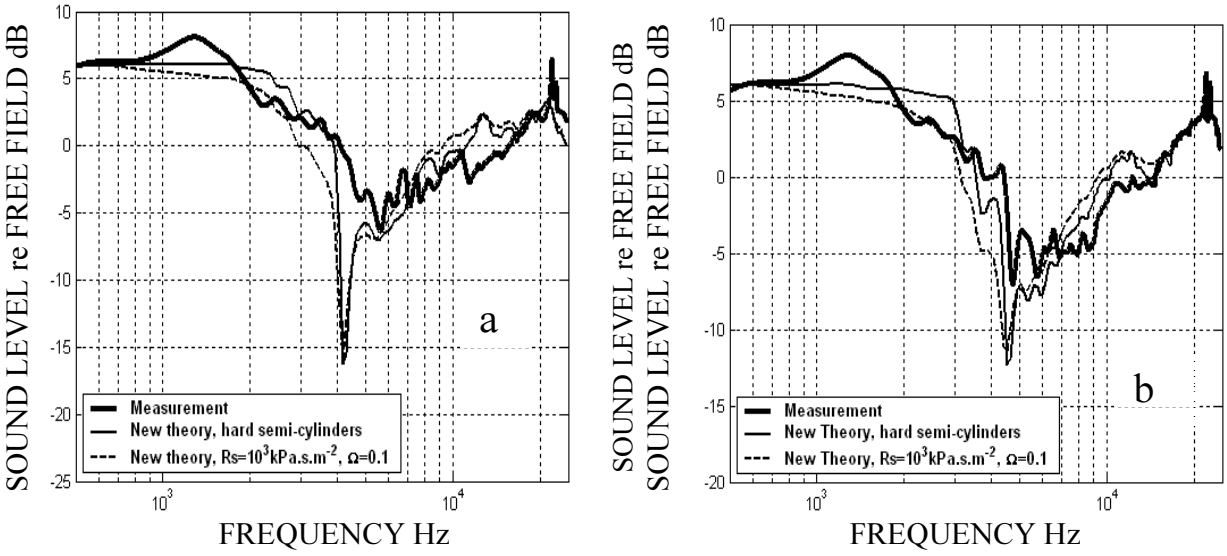

Figure 6 Predictions of the new theory for acoustically hard semi-cylinders (thin solid line), slightly porous (R_s =10^3 kPa.s.m^{-2}, Ω=0.1) semi-cylinders (dashed line) and measured (thick solid line) relative SPL spectra over random distributions of nine semi-cylinders corresponding to (a) row 2 and (b) row 3 in Table 2.

The upper frequencies determined by the truncation parameter M required by the new theory have been established for values up to M = 5. This value of M enables very good agreement between theory and experiment up to the highest measured frequency (25 kHz). Additional computations not reported here show that M = 4 gives high frequency results as good as those obtained with M = 5. However, in this study, there is no real necessity for minimizing M since the small number of semi-cylinders (9) means short run times (a few seconds) even for M = 5.

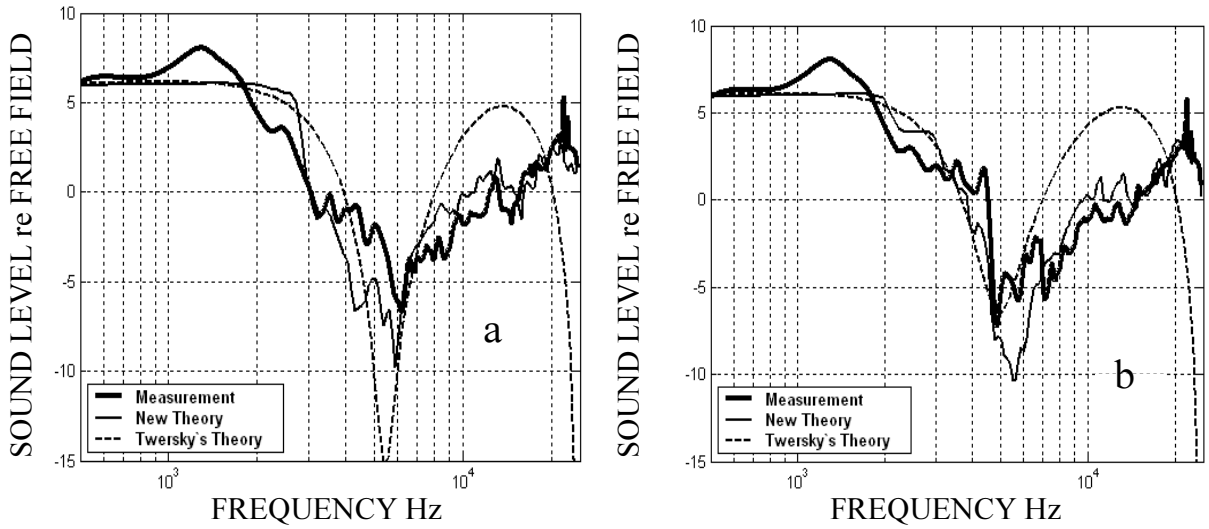

Figure 7 Predictions of the new theory (thin solid line), Twersky's theory (dashed line) and measured (thick solid line) relative SPL spectra over random distributions of nine semi-cylinders corresponding to (a) row 4 and (b) row 5 in Table 2.

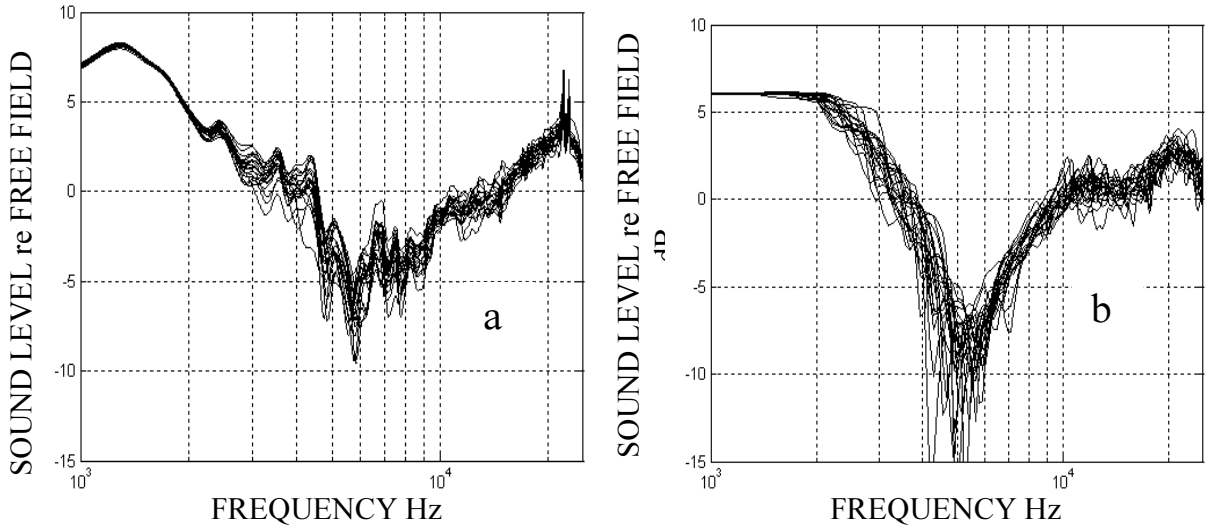

Figure 8 Measured (a) and predicted (b) relative SPL spectra over all twenty random distributions of nine semi-cylinders (Table 2).

Different relative SPL spectra are measured for different distributions of semi-cylinders with identical roughness density (see Figures 5, 6 and 7). The new theory seems to predict most of the differences. On the other hand, boss theories [1-7] predict identical results for distributions having the same roughness density. Twersky's theory [8,14] will predict different results for distributions having the same roughness density as long as the sizes of the exclusion region around a scatterer b^* are different. Examples are shown in Figure 7. But the agreement with measured data is not as good as that obtained with the new theory, particularly above 7kHz. This is in accordance with the approximation $ka < 1$, which implies for the given semi-cylinder radii, that Twersky's theory is valid only up to about 5kHz. Twersky's theory predicts the ground effect dip frequency relatively well but predicts neither the correct magnitude of the dip nor the measured oscillations.

4.2. Comparison with BEM calculations.

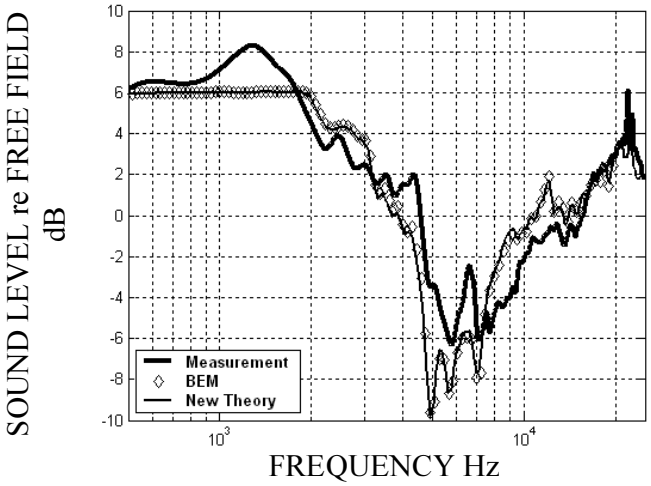

Figure 9 Predictions from the new theory (thin solid line), the BEM (diamonds) and measured (thick solid line) relative SPL spectra over the random distribution of nine semi-cylinders corresponding to row 20 in Table 2.

Figure 9 shows results of calculations using the BEM. The thick solid line represents the relative SPL spectrum measured over the twentieth random deterministic distribution of semi-cylinders. The diamonds and the thin solid line show the predictions from use of the BEM and the new theory respectively. The BEM results are based on 106 frequency points between 500Hz and 20kHz with 9 discretizing node points per semi-cylindrical profile. The BEM prediction of a single spectrum took 33 minutes of cpu time on a standard PC. Figure 9 shows predictions of the new theory also. These are more or less identical (i.e. to within 0.2 dB) to the results of BEM calculations over the entire frequency range studied. It seems that use of a truncation parameter value as low as $M = 4$, i.e. a run time of 6 seconds on a PC, is sufficient for the new theory to yield good predictions up to 20 kHz of the sound field above nine semi-cylinders. In other words, on a standard PC, the new theory achieves the same results as the BEM in $1/300^{th}$ of the time. Despite being more computationally demanding, BEM calculations could be used as an alternative to the method described in section II.C to ascertain the upper frequency of validity of the new theory for given values of the truncation parameter.

Measured data and predictions for sound reflection from a rough surface composed of sparse arrays of semi-cylindrical bosses show considerable sensitivity to the actual distribution of roughness i.e. the exact location of each roughness element. The question arises (of how many sample distributions are needed to arrive at an average representative of reflection from a non-deterministic random distribution of given roughness density? Also, how sensitive are predictions to the exact roughness density? These questions are addressed in the following section.

4.3. Average predictions for random deterministic semi-cylinder distributions

Figure 10(a) shows three 5-spectra averages (dotted, dot-dashed and dashed lines) measured over random distributions of 9 semi-cylinders compared to an average over twenty measured spectra (solid line). All of the curves are very similar. In Figure 10(b), three 5-spectra average predictions from the new theory (dotted, dot-dashed and dashed lines) are compared to a 20-predicted-spectra average (thick solid line). The predicted 5-spectra averages are not based on the same roughness distributions as those used in the average of 20 predicted spectra, whereas the measured averages are based on the same roughness distributions as those used in the 20-measured-spectra average. In spite of this, the measured 5-spectra averages do not show better agreement with the 20-measured-spectra average than is the case for the predictions. The predicted averages agree well with measured averages over the whole frequency range. The

ground effect dip frequency of the measured 20-spectra average is near 5700Hz while the corresponding prediction is near 5300Hz. The dip magnitude is predicted to be −8.6dB and the measured dip magnitude is −6.5dB for the 20-spectra averages. Comparison of the predicted averages with the exact solution for a flat hard surface (thin solid line) with identical geometry in Figure 10(b) shows that the semi-cylindrical roughness elements have a clear influence on ground effect.

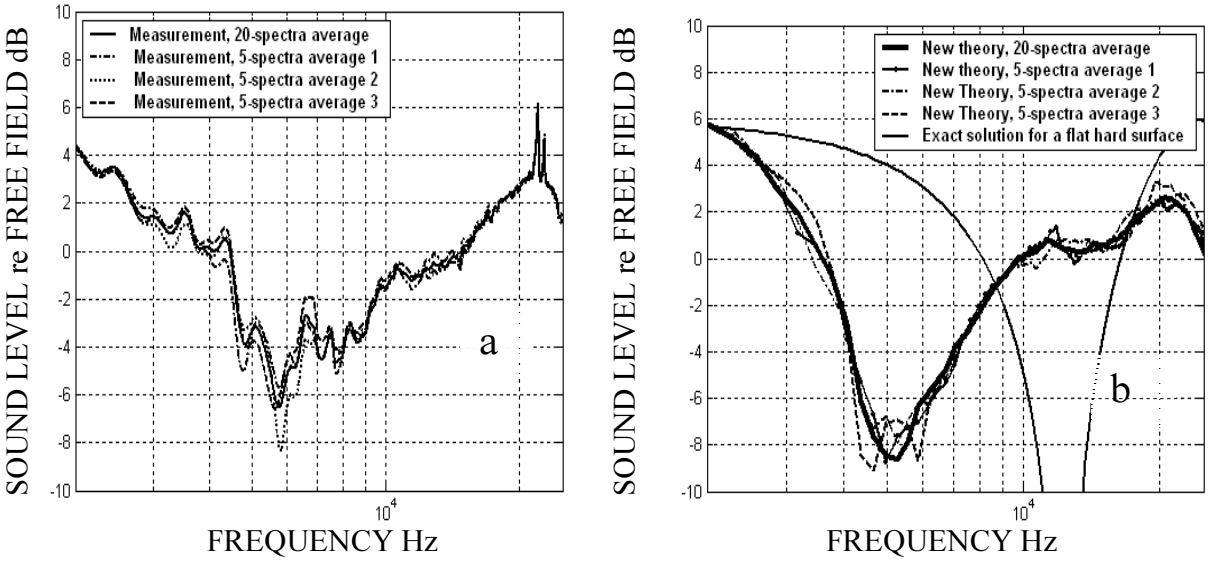

Figure 10 Comparison between 5- and 20-spectra averages of relative SPL over nine acoustically hard semi-cylinders (a = 1 cm) (a) using measurements and (b) using new theory predictions.

Figure 11 shows measured relative SPL spectra averaged over five random distributions of 12 varnished wooden 2cm-radius semi-cylinders on a flat hard surface (thick solid line) compared to the new theory predictions for (a) 5-spectra averages and (b) 20-spectra averages. The source/receiver distance is 1 m and the source/receiver heights are 10cm. More details about the experimental background and comparisons of these data with BEM calculations and boss theory predictions may be found elsewhere [9]. Comparisons of the agreement of predictions with these 'old' data and the new data reveal the consequences of normalized and non-normalized random intervals between semi-cylinders. The new data (in Figures 5 – 9) result from nine semi-cylinders being randomly distributed over 49 cm centered on the specular reflection point such that the first and ninth semi-cylinders are placed exactly at both ends of the chosen 49 cm-long segment of rough surface. However, for the older data [9], the twelve semi-cylinders were not distributed about the specular reflection point. As a result the 12th semi-cylinder was located either beyond the 1m source-receiver horizontal range or at less than 1m from the first. Two 5-spectra and 20-spectra average predictions, assuming normalized distributions of twelve 2cm-radius semi-cylinders, are shown as the dashed and thin solid lines in Figure 11(a) and 11(b) respectively. Although the exact locations of the semi-cylinders used for the earlier data are not known, their non-normalized distributions are modeled such that the 12th semi-cylinder is positioned at (1 ± 0.06) m from the first roughness, i.e. there is uncertainty of ±0.06 m due to the random interval generation. In Figures 11(a) and 11(b) show two sets of predictions. The dot-dashed and dotted lines represent results for non-normalized separations and the dashed and thin solid lines represent results for normalized random distributions. They show quite different ground effect dip frequencies and magnitudes. Nevertheless, neither assumption gives predictions close to the measured data. The result of using non-normalized distributions of semi-cylinders is that no pair

of distributions has exactly the same roughness density. For example, a density of 12/(1m –0.06m) = 0.128 cm^{-1} is obtained when the last semi-cylinder falls inside the source-receiver separation and the density is 12/(1m +0.06m) = 0.113 cm^{-1} when the last semi-cylinder falls outside the source-receiver separation. In previous work [9], these two densities were considered to be approximately equal to the average density 12/(1m) = 0.12 cm^{-1}. However, Figure 11 shows that a ±7% variation in roughness density leads to considerable differences in predicted relative SPL spectra. Consequently, the measured and predicted spectra averages based on these non-normalized distributions of semi-cylinders are not consistent with a fixed roughness density and their comparison is suspect. This suggests an explanation for the relatively poor agreement between predictions and average measured data reported previously [9]. Note also that, according to Figures 11(a) and 11 (b) for the normalized distributions of twelve 2cm-radius semi-cylinders, as well as for the normalized distributions of nine 1cm-radius semi-cylinders (Figure 10), increasing the number of distributions for averaging from five to twenty has no effect on the predicted results.

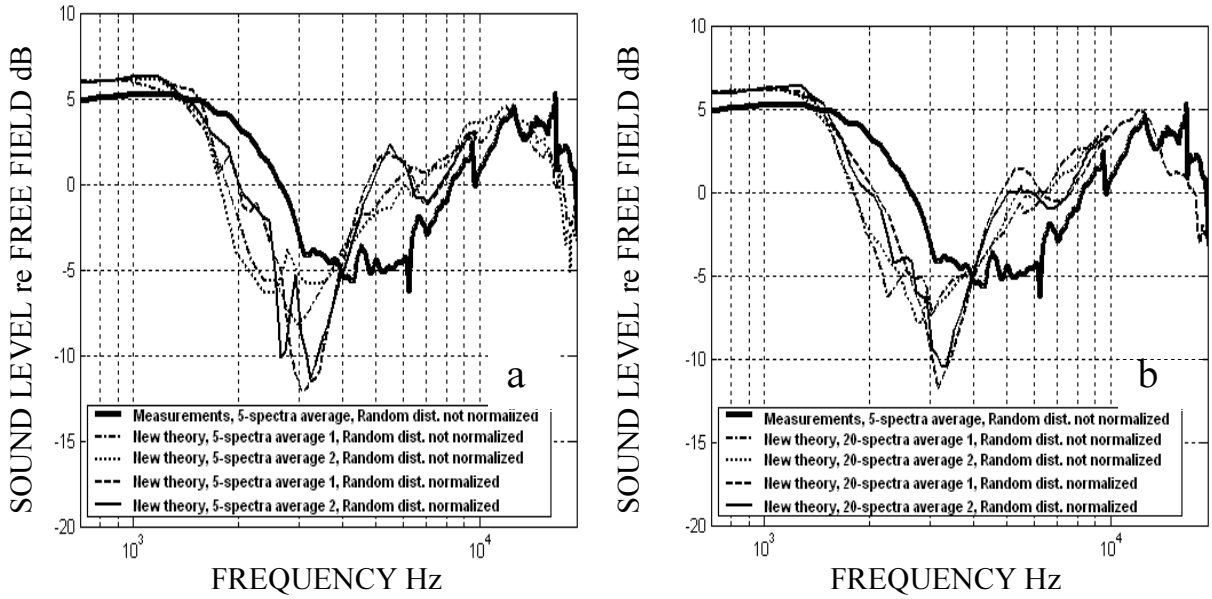

Figure 11 Comparison between the new theory predictions for (a) 5-spectra and (b) 20-spectra averages of relative SPL over twelve acoustically hard semi-cylinders (a=2cm) with a 5-spectra average data over 2cm–radii semi-cylinders (data first reported in reference 9).

5. Conclusions

A new theory has been developed that enables predictions of relative SPL spectra in good agreement with measurements over deterministic random distributions of nine wooden semi-cylinders on a glass plate. This analytical theory is more accurate than boss models [6]-[8], [12] for modeling reflection from rough surfaces. Most boss models are long-wavelength approximations. Moreover they are applicable only to non-deterministic random distributions, since the positions of the roughness elements are not included in these theories and the roughness distributions are characterized only by their number per unit area. Although the boss theory from Twersky [14] enables the modeling of roughness distributions having different radii of exclusion region around the scatterers, it does not give as good predictions as the new theory. Even when limited to an upper frequency bound by the choice of the truncation parameter, the new theory shows much better high frequency agreement with measured data than Twersky's theory which requires a small *ka* approximation. The model predicts that relative SPL spectra above rough

surfaces are very sensitive to roughness density. For example, results are significantly different when the density is increased or decreased by 7%. This means that normalizing the distribution of random roughness positions is necessary to get meaningful results that are representative of a given roughness density. When considering different measured and modeled deterministic random semi-cylindrical distributions with identical roughness density, averaging the relative SPL spectra over five distributions has been found to improve the agreement between theory and data and sufficient to obtain an average representative of the roughness density studied. Use of a truncation parameter value as low as 4 in the new theory gives predictions that are identical to within less than a dB over the entire frequency range studied (500 Hz to 20 kHz) to those obtained numerically using a BEM. For the case reported here, the new theory is found to be more than 300 times faster than the BEM to achieve the same results. Extension of the new theory to 3-D roughness is underway.

6. References

[1] Attenborough K and Taherzadeh S 1995 Propagation from a point source over a rough finite impedance boundary *J. Acoust. Soc. Am*. **98** 17 - 22

[2] Chambers J P, Raspet R and Sabatier J M 1996 Incorporating the effects of roughness in outdoor sound propagation models *Noise Con*

[3] Berthelot Y H and Chambers J P 1996 On the analogy between sound propagation over a rough surface and sound propagation over a smooth surface with modified surface impedance *Seventh international Symposium on Long-Range Sound Propagation*, Lyon, France

[4] Chambers J P and Y. H. Berthelot 1997 An experimental investigation of the propagation of sound over a curved rough, rigid surface *J. Acoust. Soc. Am.* **102**, 707 - 714

[5] Chambers J P, Sabatier J M and Raspet R 1997 Grazing incidence propagation over a soft rough surface *J. Acoust. Soc. Am.* **102** 55 - 59

[6] Tolstoy I 1982 Coherent sound scatter from a rough interface between arbitrary fluids with particular reference to roughness element shapes and corrugated surfaces *J. Acoust. Soc. Am.* **72** 960-972

[7] Tolstoy I "Smoothed boundary conditions, coherent low-frequency scatter, and boundary modes" J. Acoust. Soc. Am. **75** 1 - 22 (1984).

[8] Lucas R J and Twersky V 1984 Coherent response to a point source irradiating a rough plane" J. Acoust. Soc. Am. **76** 1847 - 63

[9] Boulanger P, Attenborough K, Taherzadeh S, Waters-Fuller T and Li K M 1998 Ground Effect Over Hard Rough Surfaces *J. Acoust. Soc. Am.* **104** 1474 - 82

[10] Attenborough K and Waters-Fuller T 2000 Effective impedance of rough porous ground surfaces *J. Acoust. Soc. Am.* **108** 949 - 956

[11] Boulanger P and Attenborough K 2005 Effective impedance spectra for predicting rough sea effects on atmospheric impulsive sounds *J. Acoust. Soc. Am.* **117** 751 – 62

[12] Boulanger P, Attenborough K, and Qin Q 2005 Effective impedance of surfaces with porous roughness: models and data *J. Acoust. Soc. Am.* **117** 1146 – 56

[13] Taherzadeh S and Attenborough K 1999 Deduction of ground impedance from measurements of excess attenuation spectra *J. Acoust. Soc. Am.* **105** 2039 - 42

[14] Twersky V 1983 Reflection and scattering of sound by correlated rough surfaces *J. Acoust. Soc. Am.* **73** 85 - 94

[15] Allard J-F *Propagation of Sound in Porous Media* 1993 Elsevier Applied Science, New York

[16] Attenborough K 1993 Models for the acoustical properties of air-saturated granular media *Acta Acustica* **1**, 213 - 226

[17] Linton C M and Evans V 1990 The interaction of waves with arrays of vertical circular cylinders *J. Fluid. Mech.* **215** 549 - 69

[18] Linton C M and Martin P A 2005 Multiple scattering by random configurations of circular cylinders: second-order corrections for the effective wave number *J. Acoust. Soc. Am.* **117** 3413 – 23

[19] IMSL math library User's Manual, Version 3.0, Visual Numerics, Inc., Houston, Texas (1994).

[20] Twersky V 1950 On the Non-Specular Reflection of Plane Waves of sound *J. Acoust. Soc. Am.* **22** 539 - 46

[21] Gradshtein I S and Ryzhik I M 1980 *Tables of Integrals, Series, and Products* Academic Press p 973 equation MO27

[22] Gradshtein I S and Ryzhik I M 1980 *Tables of Integrals, Series, and Products* Academic Press p 979, equation WA394 (6)

[23] Chien C F and Soroka W W 1975 Sound propagation along an impedance plane *J. Sound Vib.* **43** 9 – 20

[24] Chandler-Wilde S N and Hothersall D C 1995 Efficient calculation of the green function for acoustic propagation above a homogeneous impedance plane *J. Sound and Vib*. **180** 705 - 24

[25] Chandler-Wilde S N and Hothersall D C 1995 A uniformly valid far field asymptotic expansion of the green function for two-dimensional propagation above a homogeneous impedance plane *J. Sound and Vib.* **182** 665 - 675